PERGAMON

Transportation Research Part B 37 (2003) 207–223

TRANSPORTATION RESEARCH PART B

www.elsevier.com/locate/trb

The formation and structure of vehicle clusters in the Payne–Whitham traffic flow model

W.L. Jin, H.M. Zhang *

Civil and Environmental Engineering, University of California, 156 Everson Hall, Davis, CA 95616, USA

Received 17 October 2001; received in revised form 28 December 2001; accepted 8 January 2002

Abstract

In this paper, we study the Payne–Whitham (PW) model as a hyperbolic system of conservation laws with relaxation and are interested in its solution patterns when it is unstable. With numerical simulations, we observed the formation of clusters in the solutions. A cluster, which consists of a shock and a transition layer, is a "strong" traveling wave in the sense of Liu (Commun. Math. Phys. 108 (1987) 153), and its traveling speed is equal to that of the corresponding shock. The time-asymptotic structure of a transition layer is described by a first-order ordinary differential equation. We also found that, due to the instability of the PW model, we could not predict the number of clusters or the position, height, or width of each cluster. Our study also reveals the intricate relationship between the structure of vehicle clusters and the parameter c_0.

Keywords: The Payne–Whitham model; Hyperbolic system of conservation laws with relaxation; Strong traveling waves; Cluster; Transition layer

1. Introduction

Continuum models of vehicular traffic on long crowded roads, which is simpler in both computation and storage compared with microscopic models, are largely used in the study of traffic phenomena and management of traffic system. In these models, traffic conditions at location x and time t can be measured by three aggregate values: traffic density ρ, travel speed v, and flow rate $q = \rho v$. Certain relationship has been observed among ρ, v, and q in equilibrium traffic. For example, v is non-increasing in ρ, $q = 0$ when $\rho = 0$ or ρ_j (the jammed density), and q attains its

* Corresponding author. Tel.: +1-530-754-9203; fax: +1-530-754-7872.
E-mail address: hmzhang@scarlet.ucdavis.edu (H.M. Zhang).

0191-2615/03/$ - see front matter
PII: S0191-2615(02)00008-5

maximum (the capacity) for a critical ρ. Therefore, one may assume that there exists a function of q in ρ, $q = f_*(\rho)$, which is called the fundamental diagram; correspondingly we have the speed–density relationship $v = v_*(\rho) \equiv f_*(\rho)/\rho$. Examples of the fundamental diagram can be found in Newell (1993) and Kerner and Konhäuser (1994). Generally, the equilibrium velocity is assumed to be decreasing with respect to density; i.e., $v'_*(\rho) < 0$; the equilibrium flow rate is concave; i.e., $f''_*(\rho) < 0$.

In continuum models, conservation of traffic is the basic principle described by a partial differential equation,

$$\rho_t + q_x = 0. \tag{1}$$

The above equation for equilibrium traffic becomes the LWR model suggested by Lighthill and Whitham (1955) and Richards (1956) and can be written as

$$\rho_t + (\rho v_*(\rho))_x = 0. \tag{2}$$

To model non-equilibrium traffic, Payne (1971) and Whitham (1974) suggested the PW model, in which another equation is introduced to capture the change of velocity,

$$v_t + v v_x + \frac{c_0^2}{\rho}\rho_x = \frac{v_*(\rho) - v}{\tau}, \tag{3}$$

where the constant $c_0 > 0$ is the traffic sound speed and τ is the reaction time or relaxation time. Setting $q = \rho v$, the PW model can be written as

$$\begin{pmatrix} \rho \\ q \end{pmatrix}_t + \begin{pmatrix} q \\ \frac{q^2}{\rho} + c_0^2\rho \end{pmatrix}_x = \begin{pmatrix} 0 \\ \frac{f_*(\rho)-q}{\tau} \end{pmatrix}, \tag{4}$$

which can be rewritten as

$$U_t + f(U)_x = s(U), \tag{5}$$

where $U = (\rho, q)$ is the state of traffic flow, and $s(U)$ is the source term or relaxation term. Thus the PW model is a "system of hyperbolic conservation laws with relaxation" in the sense of Whitham (1959, 1974) and Liu (1987).

The two wave velocities of the system (4), $\lambda_{1,2}$, are the eigenvalues of $\partial f(U)$; i.e., $\lambda_{1,2} = v \mp c_0$. It has been shown (Schochet, 1988) that the PW model approaches the viscous version of the LWR model, $\rho_t + (\rho v_*(\rho))_x = v\rho_{xx}$, as $\tau \to 0$. Hence the LWR model is generally called the subsystem of (4), and the wave velocity of the LWR model, $\lambda_*(\rho) = v_*(\rho) + \rho v'_*(\rho)$, is called the subcharacteristic of the PW model.

Different from the LWR model, however, the PW model can be unstable. Whitham (1959, 1974) showed that the stability condition for the linearized system with a relaxation term is

$$\lambda_1 < \lambda_* < \lambda_2. \tag{6}$$

When the PW model is unstable, Kerner and Konhäuser (1994) observed cluster solutions, but the PW model they studied has a viscous term $v v_{xx}/\rho$ in the right hand side of (3), for which the numerical computation is much more costly than for the PW model without the viscous term. It is suspected that cluster solutions also exist in the PW model (Zhang, 1999) when traffic is unstable. Using the numerical solution method for (4) (Jin and Zhang, submitted to Transport. Res.), we

will investigate, both numerically and analytically, solutions to the PW model when it is unstable. In this paper, we show the solution patterns of the PW model when initial conditions are unstable. Besides, analysis of the time-asymptotic solutions will also be carried out.

This paper is organized as follows. In Section 2, we review the numerical method for solving the PW model, present the fundamental diagram, and perform instability test for the PW model. In Section 3, the formation of cluster solutions to the PW model are discussed and the structure of clusters is analyzed. In Section 4, the appearance of clusters with respect to different factors is studied. In Section 5, we conclude our findings, compare them with those by Kerner and Konhäuser, and suggest further study directions.

2. Preliminaries

2.1. The ring road, fundamental diagram, and initial traffic conditions

In this paper, we study the PW model for a single-lane ring road, with length $L = 800l$, over the time interval $[0, T_0]$, where $T_0 = 500\tau$. Here $l = 0.028$ km and the relaxation time $\tau = 5$ s. In the numerical studies, we partition the roadway into N cells and the time interval into K steps, with $N/K = 1/8$; e.g., if $N = 100$ and $K = 500$, the cell length is $\Delta x = 8l$ km and the length of each time step $\Delta t = 0.625\tau$ s.

For the fundamental diagram, the model parameters are chosen as follows (Kerner and Konhäuser, 1994; Herrmann and Kerner, 1998): the free flow speed $v_f = 5l/\tau$, the jam density $\rho_j = 180$ veh/km, and the sound speed $c_0 = 2.48445l/\tau$; the equilibrium speed–density relationship $v_*(\rho) = 5.0461[(1 + \exp\{[\rho/\rho_j - 0.25]/0.06\})^{-1} - 3.72 \times 10^{-6}]l/\tau$. The equilibrium functions $v_*(\rho)$ and $f_*(\rho)$ are given in Fig. 1, in which the two critical densities $\rho_{c1} = 0.173\rho_j = 31$ veh/km and $\rho_{c2} = 0.396\rho_j = 71$ veh/km, determined by $\rho v_*'(\rho) + c_0 = 0$. Since $\lambda_2 \leqslant v_f + c_0 < 7.5l/\tau$, we find that the CFL (Courant et al., 1928) condition number $\lambda_2 \Delta t/\Delta x \leqslant 0.5859 < 1$.

Two types of initial traffic conditions will be used: One is a non-equilibrium global perturbation,

$$\begin{aligned} &\rho(x,0) = \rho_h + \Delta\rho_0 \cos(2\pi x/L), \quad x \in [0, L], \\ &v(x,0) = v_*(\rho_h) + \Delta v_0 \cos(2\pi x/L), \quad x \in [0, L]; \end{aligned} \tag{7}$$

the other is an equilibrium local perturbation,

$$\begin{aligned} &\rho(x,0) = \begin{cases} \rho_h + \Delta\rho_0 & \text{when } x \in [37.5l, 48.4l], \\ \rho_h - \Delta\rho_0/3 & \text{when } x \in [50.0l, 82.8l], \\ \rho_h & \text{otherwise}, \end{cases} \\ &v(x,0) = v_*(\rho(x,0)). \end{aligned} \tag{8}$$

For both initial conditions, the average traffic density on the ring road is ρ_h and the total number of vehicles on the ring road is always $\rho_h 800l$.

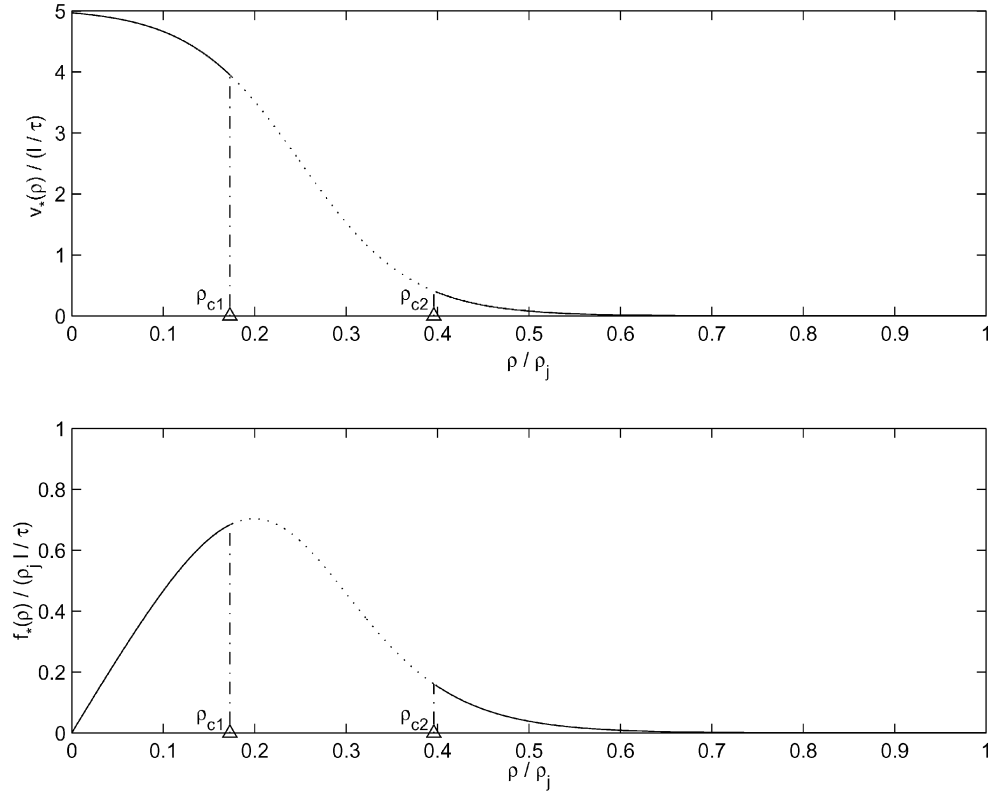

Fig. 1. The Kerner–Konhäuser model of speed– and flow–density relations.

2.2. Numerical solution method

In this section, we review the numerical solution method. For detailed discussions of the method, please refer to Jin and Zhang (submitted to Transport. Res.). In this method, first-order Godunov (1959) difference equations are used to approximate the homogeneous part of the PW model, and the source term is treated implicitly. In cell i, (5) is approximated by the following finite difference equations,

$$U_i^{j+1} = U_i^j - \frac{\Delta t}{\Delta x}\left(f(U_{i+1/2}^{*j}) - f(U_{i-1/2}^{*j})\right) + \Delta t\,\tilde{s}(U_i^{j+1}), \tag{9}$$

in which U_i^j is the average of $u(x,t)$ over ith cell at time $j\Delta t$, and $U_{i+1/2}^{*j}$ is the average at the right boundary of ith cell over time interval $[j\Delta t,(j+1)\Delta t]$. From the above equation, we can update ρ and q as follows,

$$\rho_i^{j+1} = \rho_i^j - \frac{\Delta t}{\Delta x}\left(q_{i+1/2}^{*j} - q_{i-1/2}^{*j}\right), \tag{10}$$

$$q_i^{j+1} = \frac{1}{(1+\Delta t/\tau)}\left\{q_i^j - \frac{\Delta t}{\Delta x}\left[\frac{\left(q_{i+1/2}^{*j}\right)^2}{\rho_{i+1/2}^{*j}} + c_0^2\rho_{i+1/2}^{*j} - \frac{\left(q_{i-1/2}^{*j}\right)^2}{\rho_{i+1/2}^{*j}} - c_0^2\rho_{i-1/2}^{*j}\right] + \frac{\Delta t}{\tau}f_*(\rho_i^{j+1})\right\}. \tag{11}$$

In Jin and Zhang (submitted to Transport. Res.), it is shown that the numerical method itself is convergent for initial conditions inside the stability domain of the PW model. It is also tested that the numerical method would not yield convergent solutions for unstable initial conditions, since the PW model, when it is unstable, is very sensitive to small changes in initial conditions, including those caused by different number of grids N.

3. Cluster solutions for the PW model

3.1. The formation and structure of a cluster

We first observe the formation of a cluster for the PW model with the initial condition (7), in which $\rho_h = 0.1833\rho_j = 33$ veh/km, $\Delta\rho_0 = 0.0167\rho_j = 3$ veh/km, and $\Delta v_0 = 0.2l/\tau$. When the number of grids of the ring road is $N = 200$, the contour plots of the solutions till $T_0 = 500\tau$ are given in Fig. 2, and solutions of ρ and v, and q at selected times are given in Figs. 3 and 4. These figures show the formation of the cluster as follows: (i) During $t = 0$ and $t = 150\tau$, a forward shock forms in the region $[400l, 800l]$, a rarefaction in $[0l, 400l]$, and during 20τ and 120τ, a U-shaped region forms in the region from $x = 710l$ to $x = 110l$, in which the velocities of rarefaction waves are near 0, i.e., the discharging flow inside this region is low. (ii) Due to the upstream forward shock wave and the low discharging flow, the traffic density inside the U-shaped region

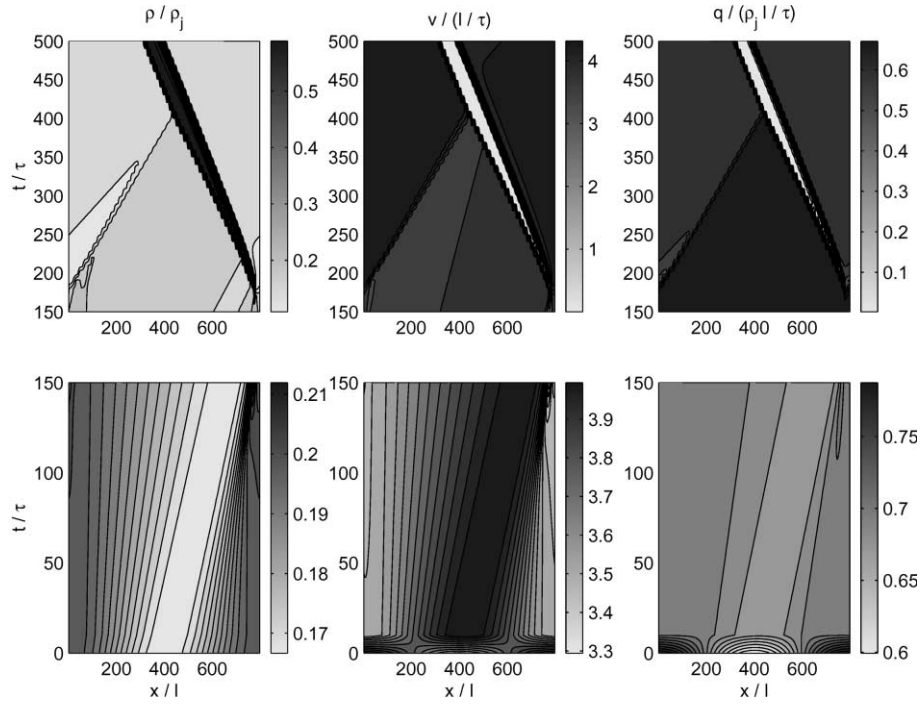

Fig. 2. The formation of a cluster for initial condition (7).

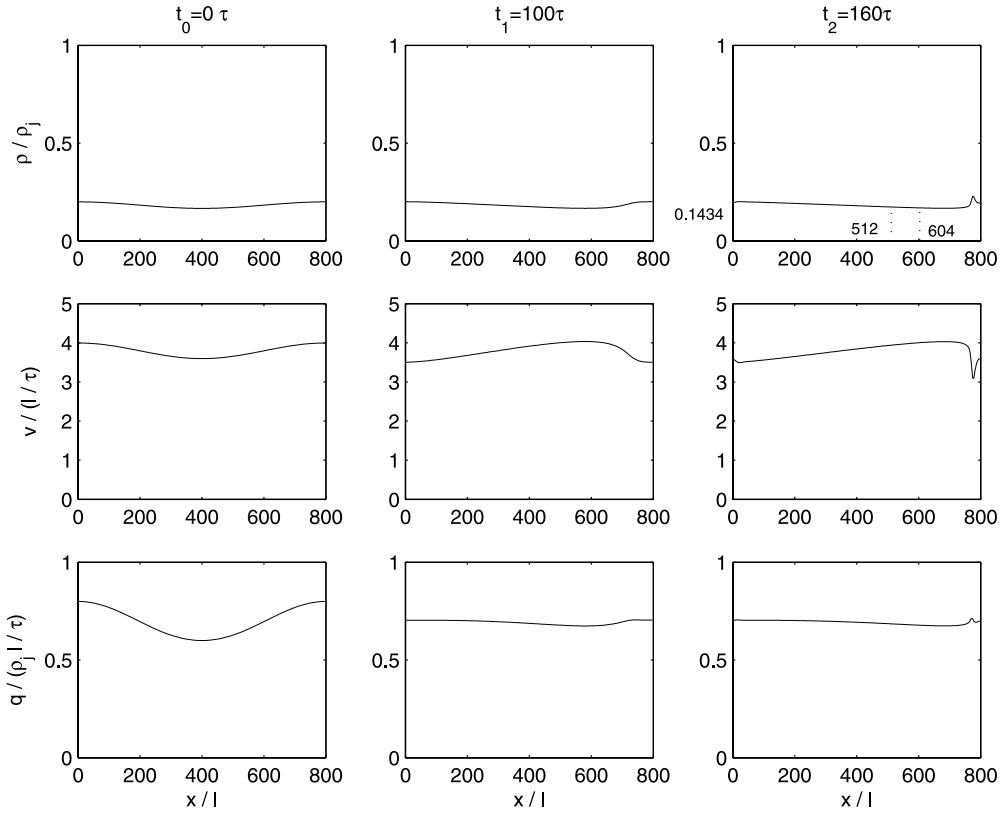

Fig. 3. Solutions in Fig. 2 at 0τ, 100τ, and 160τ.

keep increasing and finally, at $t = 130\tau$, a clearly visible local cluster forms at around $x = 780l$. (iii) Starting from $t = 150\tau$, the maximum density of the cluster grows high enough that a backward shock forms, and the cluster keeps absorbing the rarefaction wave. (iv) At $t = 400\tau$, the forward rarefaction totally disappears and a stable cluster forms and moves backward in a constant speed $a \approx -1.36l/\tau$. Indeed the cluster is a traveling wave.

The process of the formation of the cluster can also be shown by solutions at different times in the phase plane, given in Figs. 5 and 6. From Fig. 6, we can see that the stable cluster is not in equilibrium, i.e., $v \neq v_*(\rho)$ for traffic in the cluster. This figure, in which the arrow indicates the increasing direction of x, also shows the structure of the cluster. That is, the cluster consists of two important states, the peak point B with the highest density $\rho_B = 0.6004\rho_j$ and the homogeneous free flow state A with $\rho_A = 0.1423\rho_j$, both of which are in equilibrium. In the cluster, a shock wave (described in the figure by several transition states) connects the peak point B to the homogeneous free flow state A from the left, and a transition layer containing a larger number of transition states in the figure connects B to A from the right. The transition layer, as shown in Fig. 4, is smooth. In Fig. 6, we can also see that the speed of the left shock is equal to the slope of the line AB. Since the cluster is stable (which means no interaction between the left shock and the right transition), the traveling speed of the transition layer is also the slope of the line AB. Thus the cluster solution for the PW model is a "strong" traveling wave in the sense of Liu (1987).

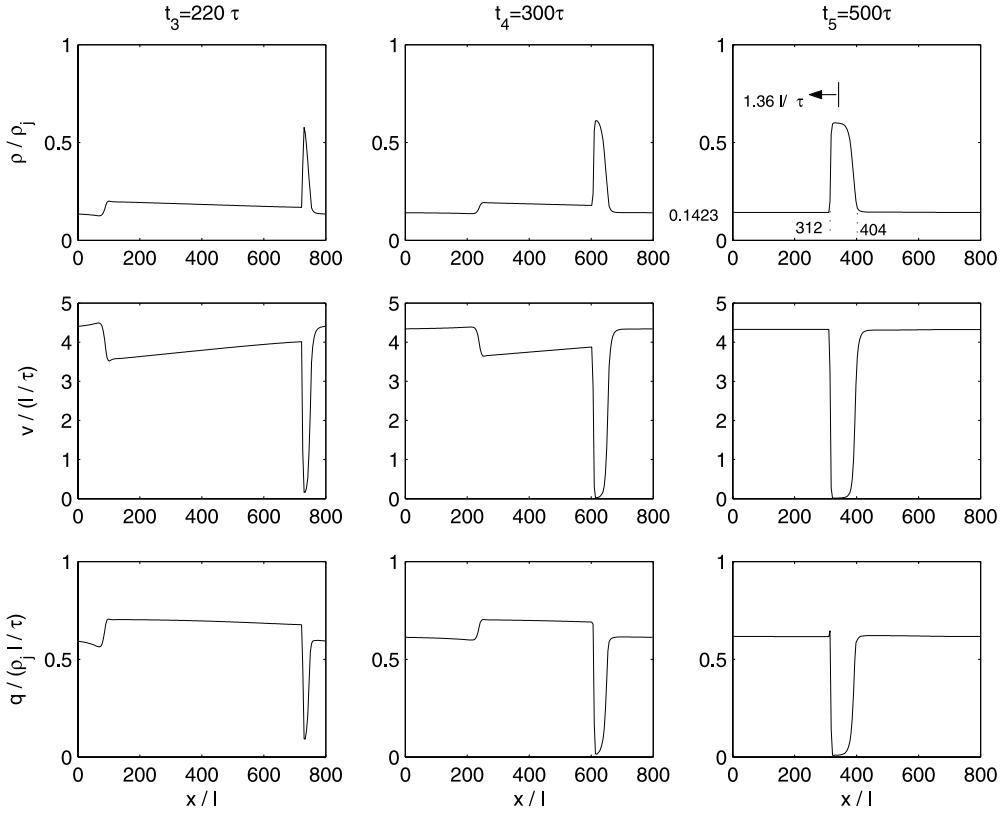

Fig. 4. Solutions in Fig. 2 at 220τ, 300τ, and 500τ.

3.2. Time-asymptotic clusters for the PW model and their structure

The observations made in the previous subsection suggest that for the PW model a certain type of time-asymptotic solutions are the traveling clusters. In this subsection, we will analyze the structural properties of the clusters.

Suppose traffic densities for the peak point B and the homogeneous free flow A are ρ_B and ρ_A respectively, then the shock wave speed can be computed as

$$a = \frac{f_*(\rho_A) - f_*(\rho_B)}{\rho_A - \rho_B}. \tag{12}$$

Then in the smooth transition layer, which travels with speed a, we can write $\rho(x,t)$ and $q(x,t)$ as $\rho(x,t) = \rho(\xi)$ and $q(x,t) = q(\xi)$, where $\xi = x - at$. Since $\rho_t = -a\rho', \rho_x = \rho', q_t = -aq'$, and $q_x = q'$, we obtain from (4)

$$-a\rho' + q' = 0, \tag{13}$$

$$\left(-a + 2\frac{q}{\rho}\right)q' + \left(c_0^2 - \frac{q^2}{\rho^2}\right)\rho' = \frac{f_*(\rho) - q}{\tau}. \tag{14}$$

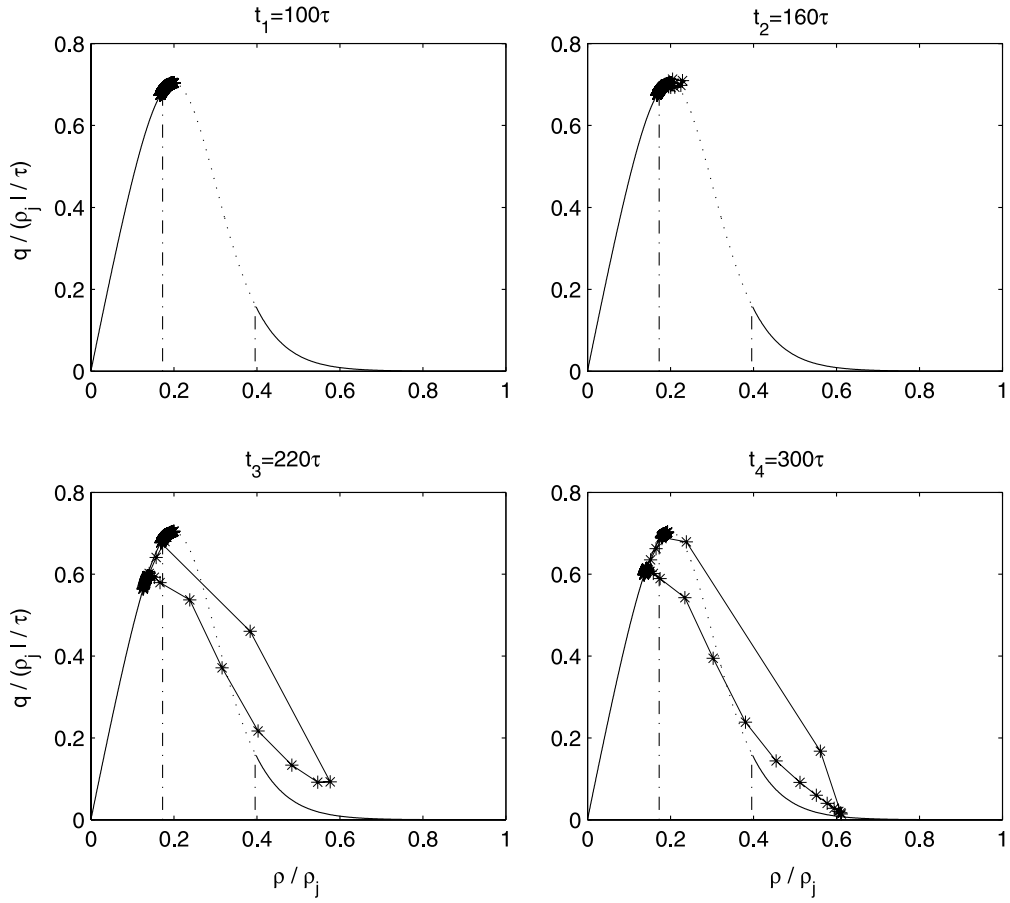

Fig. 5. Solutions in Fig. 2 at 100τ, 160τ, 220τ, and 300τ in the ρ–q plane.

From (13), we have

$$q = a\rho + q_0, \tag{15}$$

where q_0 is a constant with respect to ξ, therefore, x and t. Since the starting point of the transition layer is B and the ending point of the transition layer is A, we then have

$$q_0 = f_*(\rho_A) - a\rho_A = f_*(\rho_B) - a\rho_B. \tag{16}$$

From the above equation and (15) we can see that, in the traveling clusters, states in the transition layer lie on a line segment in the ρ–q phase plane, which starts from the peak point and ends at the homogeneous traffic state.

Plug (15) into (14), we have another equation for the transition layer

$$\rho' = \frac{\rho^2(f_*(\rho) - a\rho - q_0)}{\tau(c_0^2\rho^2 - q_0^2)} \equiv g(\rho), \tag{17}$$

which is an autonomous system of ρ with respect to ξ. Fig. 6 also suggests that the transition layer and the fundamental diagram has a point of intersection, labeled as C. Then for C we have

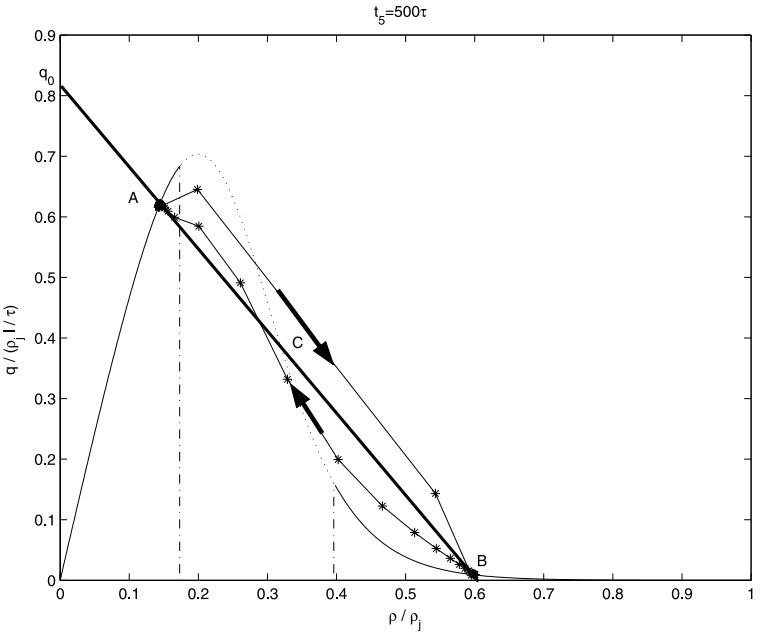

Fig. 6. Solutions in Fig. 2 at 500τ in the ρ–q plane.

$f_*(\rho_C) = q_0 + a\rho_C$. On the other hand from Fig. 4 we can see that at C $\rho_\xi < 0$, thus $g(\rho_C) \neq 0$, which means ρ_C is both a pole and singular point for $g(\rho)$; i.e., $\rho_C = q_0/c_0$. Hence we have

$$f_*(q_0/c_0) = q_0 + aq_0/c_0. \tag{18}$$

Since $g(\rho_A) = g(\rho_B) = 0$, ρ_A and ρ_B are two fixed points for the transition layer (17).

From Eqs. (12), (16), and (18), we can see that when any one of ρ_A, ρ_B, a, and q_0 is known, all the other quantities are known, and consequently the transition layer can be determined from (17). The way of determining ρ_C, q_C, a, ρ_A, and ρ_B from q_0 are shown in Fig. 7. For example, when $q_0 = 0.8\rho_j l/\tau$, we start with the point D where $q_D = q_0$ and draw a line DE whose slope is $-1/c_0$. Thus, $\rho_E = q_0/c_0 = \rho_C$. Draw a vertical line EC, which intersects with the fundamental diagram at C. Then the line DC intersects the fundamental diagram at two other points A and B, whose densities are ρ_A and ρ_B respectively. Since $\rho_B \leqslant \rho_j$ and $\rho_C \leqslant \rho_B$, the boundaries for these quantities are $0.7127 \leqslant q_0/(\rho_j l/\tau) \leqslant 0.98$, $-0.7130 \geqslant a/(l/\tau) \geqslant -2.0677$, $\rho_j \geqslant \rho_B \geqslant \rho_{c2}$, $0.2869 \leqslant \rho_C/\rho_j \leqslant 0.3945$, and $0.1410 \leqslant \rho_A/\rho_j \leqslant 0.1574$.

Setting $\rho(\xi = 0) = \rho_C$ for different q_0, we can solve (17) as an initial value problem for $\xi \in [-40l, 40l]$, and the solutions are illustrated in Fig. 8. From the solutions of the transition layer, we can see that the transition layer is very narrow and close to a jump with respect to the ring road, whose length is $800l$. Therefore, the transition layer can be considered as a rarefaction wave solution of the LWR model with a modified fundamental diagram defined as follows:

$$q = \begin{cases} q_0 + a\rho, & \rho \in [\rho_A, \rho_B]; \\ f_*(\rho), & \text{otherwise.} \end{cases} \tag{19}$$

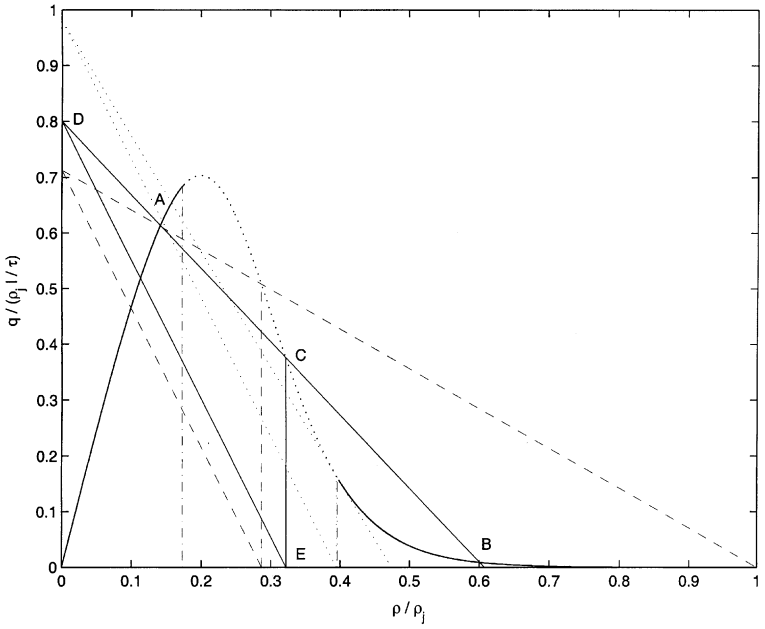

Fig. 7. Finding time-asymptotic clusters from q_0: the dashed line for $q_0 = 0.7127\rho_j l/\tau$, the solid line for $q_0 = 0.8\rho_j l/\tau$, and the dotted line for $q_0 = 0.98\rho_j l/\tau$.

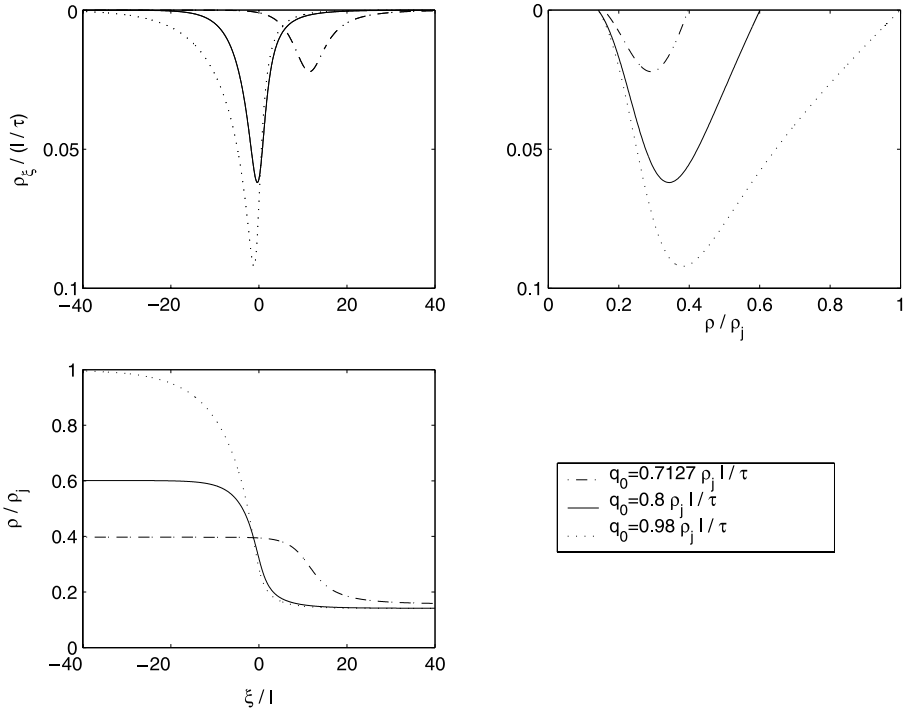

Fig. 8. The structure of transition layers.

In the traveling wave solutions for the PW model, we can not determine the number of clusters or the position of each cluster from (17). However, all possible clusters have the same ρ_A, therefore, the same ρ_B and the same structure for the transition layer. Since the transition layer is close to a jump from ρ_B to ρ_A, we define the total width w of all clusters by

$$w = \frac{\int_{\xi=0}^{800l} \rho(\xi)\,\mathrm{d}\xi - \rho_A 800l}{\rho_B - \rho_A}. \tag{20}$$

Table 1
The appearance of clusters affected by different factors

Figure	IC	ρ_h	$\Delta\rho_0$	N
9	(7)	$0.1833\rho_j$	$0.0167\rho_j$	1600 vs. 6400
10	(7)	$0.1833\rho_j$	$0.0056\rho_j$ vs. $0.0278\rho_j$	6400
11	(7)	$0.2778\rho_j$ vs. $0.3833\rho_j$	$0.0167\rho_j$	6400
12	(8)	$0.1833\rho_j$	$0.0167\rho_j$	200 vs. 1600 vs. 6400
13	(8)	$0.1833\rho_j$	$0.0056\rho_j$ vs. $0.0278\rho_j$	6400
14	(8)	$0.2778\rho_j$ vs. $0.3833\rho_j$	$0.0167\rho_j$	6400

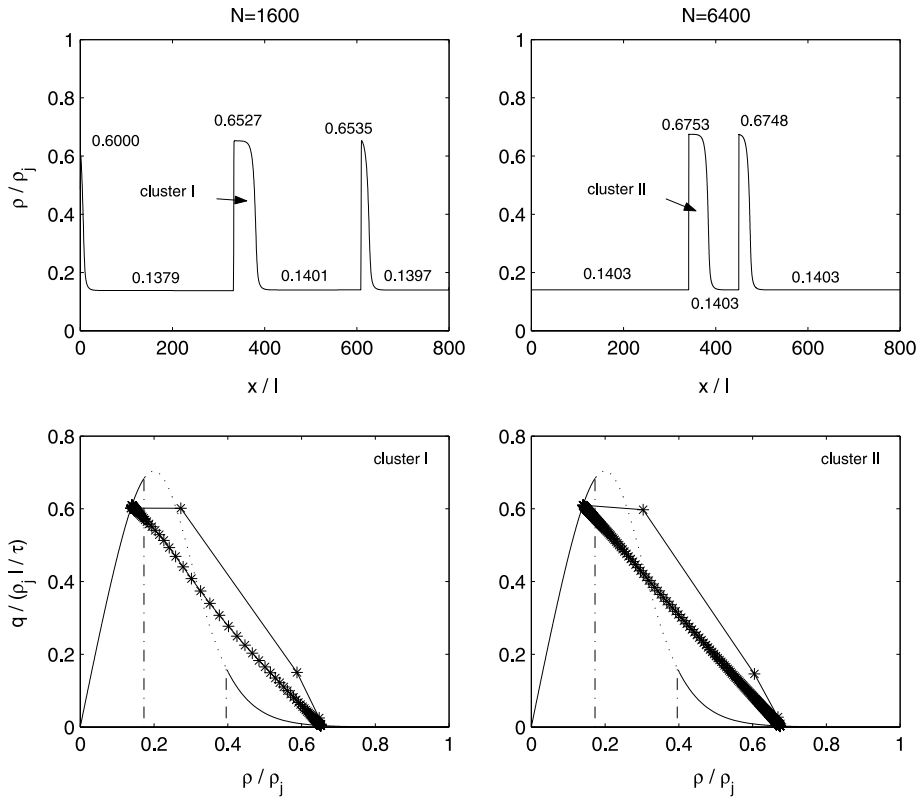

Fig. 9. Solutions with different number of grids N at 500τ for (7) with $\rho_h = 0.1833\rho_j$ and $\Delta\rho_0 = 0.0167\rho_j$.

Due to traffic conservation on the ring road, we have

$$\int_{\xi=0}^{800l} \rho(\xi)\,\mathrm{d}\xi = \rho_{\mathrm{h}}\,800l. \tag{21}$$

Therefore

$$w = \frac{\rho_{\mathrm{h}} - \rho_{\mathrm{A}}}{\rho_{\mathrm{B}} - \rho_{\mathrm{A}}}\,800l. \tag{22}$$

From the above analysis, we can see that, besides the cluster traveling waves, the "anti-cluster" (Kerner and Konhäuser, 1994) traveling waves can also be solutions to the PW model. The anti-cluster also consists of a transition layer described above and a shock wave, but the shock wave is right to the transition layer. In fact, the cluster shown in Fig. 4 can be considered as a wide anti-cluster.

4. Factors that affect the appearance of clusters

In this section, we study the factors that affect the appearance of clusters for the PW model. These factors include the type of initial conditions (IC), the initial traffic density ρ_{h}, the perturbation $\Delta\rho_0$, and the number of grids N. In each case, we will show the solutions by the graph of ρ at $t_5 = 500\tau$ vs. x and the phase plane graph of q vs. ρ. The cases are listed in Table 1 (Figs. 9–14).

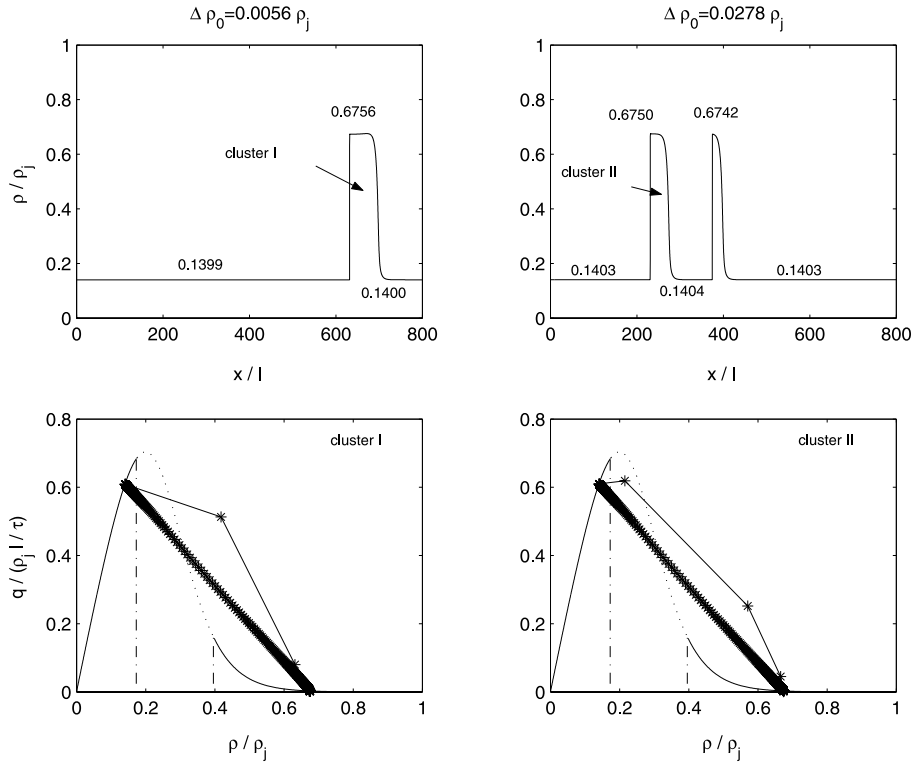

Fig. 10. Solutions with different oscillations $\Delta\rho_0$ at 500τ for (7) with $\rho_{\mathrm{h}} = 0.1833\rho_{\mathrm{j}}$ and $N = 6400$.

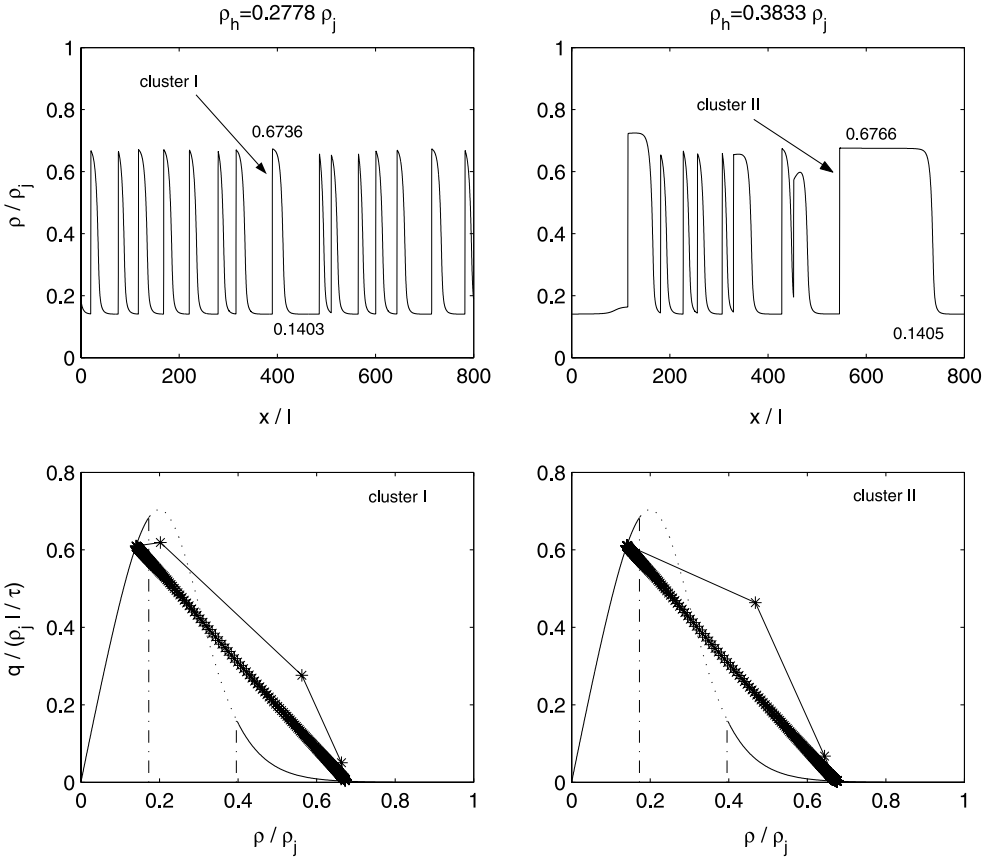

Fig. 11. Solutions with different initial traffic density ρ_h at 500τ for (7) with $\Delta\rho_0 = 0.0167\rho_j$ and $N = 6400$.

We will distinguish the influence of different factors to the appearance of clusters in the following subsections.

4.1. The number of grids N and the oscillations $\Delta\rho_0$

From Figs. 9, 4, and 6, we can see that, for the global perturbation (7), the transition layer of clusters converges to a line on the ρ–q plane when N increases. Since the traveling clusters become stable at $t_5 = 500$ when $N = 200$, 1600, and 6400, these solutions are asymptotic solutions. Hence these figures show that the numerical solutions approach the asymptotic solutions for the PW model. However, ρ_A, ρ_B, the number of clusters, and the position of each cluster may vary over different number of grids. This is because, for different number of grids, the initial conditions are in fact different although close to each other. Since the PW model is unstable for these initial conditions and, when a model becomes unstable, its solutions are very sensitive to small changes in initial data, the resulted solutions are different from each other.

Instability of the PW model can also be observed with initial conditions (8). In Fig. 12, the positions of clusters vary with respect to the number of grids. But due to the special structure of

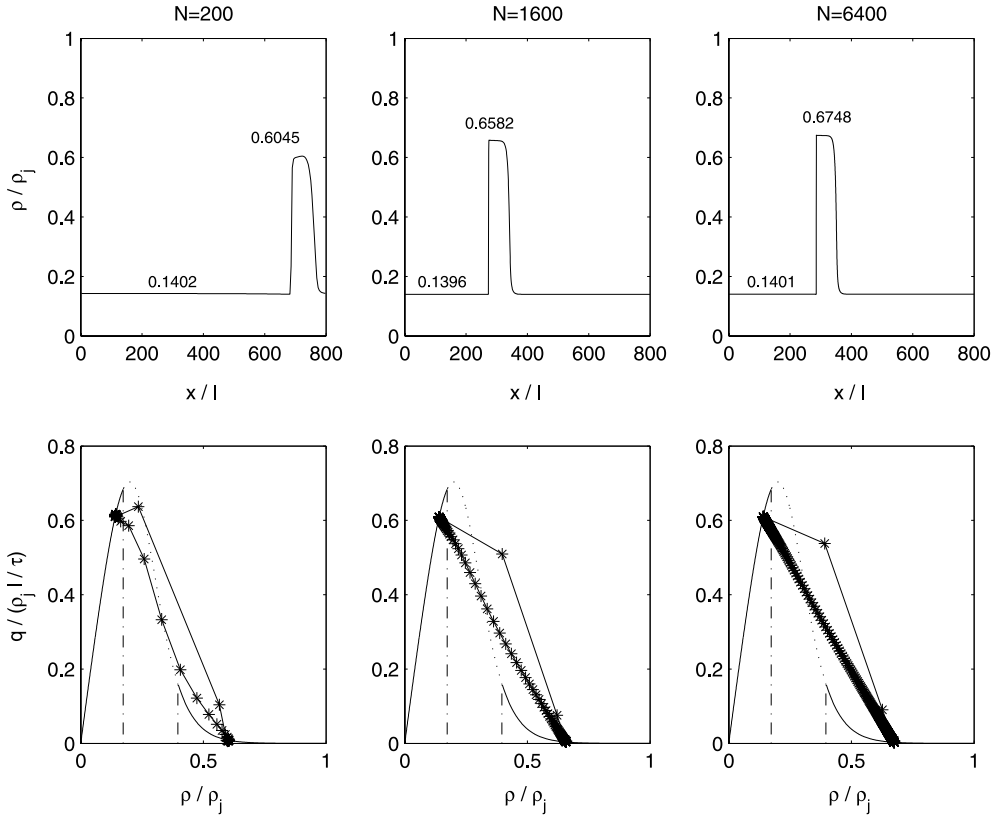

Fig. 12. Solutions with different number of grids N at 500τ for (8) with $\rho_h = 0.1833\rho_j$ and $\Delta\rho_0 = 0.0167\rho_j$.

the initial condition, when N increases, the initial conditions used by the numerical method get closer and closer, and the differences between the positions of clusters become smaller and smaller. This suggests that, if the actual initial conditions used by the numerical method are exactly the same, then the numerical solutions can still converge regardless of the instability of the PW model. That is, the numerical method is stable, and what affects the solutions is the actual initial conditions. Therefore, for any initial conditions, we can have a hint of the solution to the PW model by using sufficiently large N. But we are not certain about whether the solution is close enough to the true solution.

The oscillations $\Delta\rho_0$ have similar influence on the appearance of clusters, which are shown in Figs. 10 and 13.

4.2. The initial traffic density ρ_h

When $\rho_h = 0.2778\rho_j = 50$ veh/km, solutions at $t_5 = 500\tau$ for both initial conditions comprise of a number of stable clusters. When $\rho_h = 0.3833\rho_j = 69$ veh/km, however, solutions are not stable at $t_5 = 500\tau$, i.e., clusters still interact with each other. The interaction of clusters can be clearly seen in solutions for the local perturbation, given by the right figures in Fig. 14, in which the

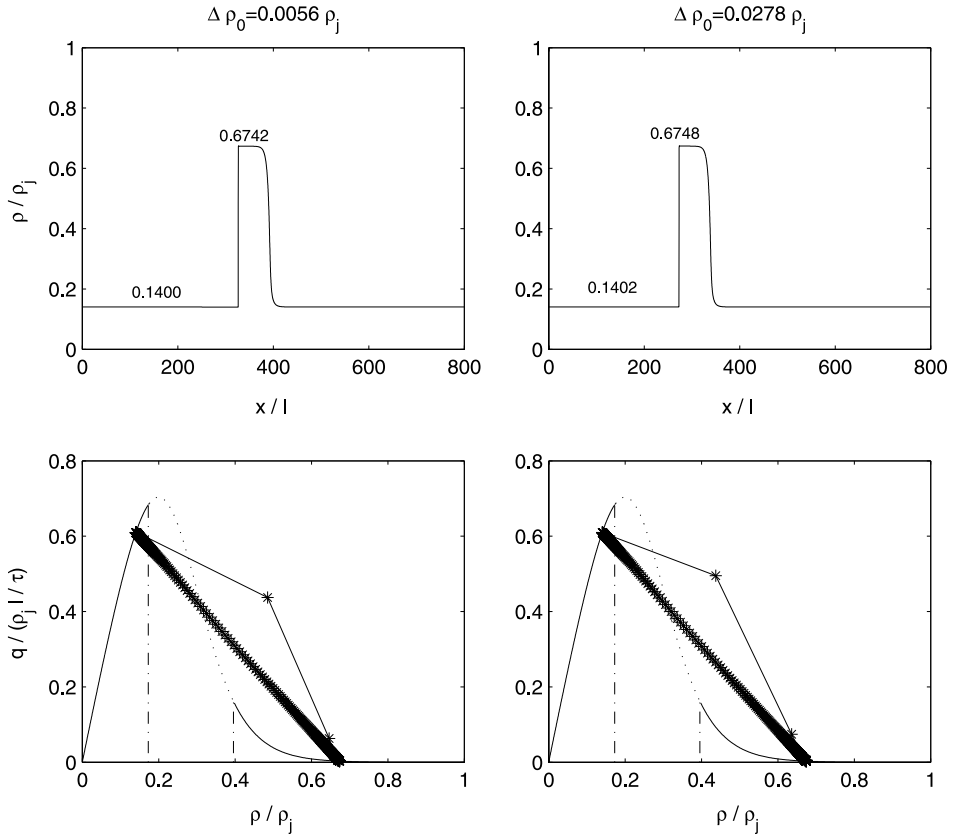

Fig. 13. Solutions with different oscillations $\Delta\rho_0$ at 500τ for (8) with $\rho_h = 0.1833\rho_j$ and $N = 6400$.

cluster consists of a left shock with speed a_3, a middle transition layer with speed a_2, and a right transition layer with speed a_1. The shock and transition layers all move backward, since $|a_2| < |a_1|$, the right transition layer will catch up with the middle one and the two transition layers will merge into one. The merge of transition layers in fact is similar to that of shocks.

5. Conclusions

In this paper, we investigate, numerically, the solution patterns of the PW model when it is unstable and find that stable strong traveling wave solutions, including clusters and anti-clusters, exist after a sufficiently long time. We show, with numerical simulations, formation of clusters and interaction between clusters. The structure of clusters is determined by Eqs. (12), (16), and (18). We also find that, due to the instability of the PW model, we can not predict the number of clusters or the position, height, or width of each cluster with numerical simulations.

Comparing the numerical results with those presented by Kerner and Konhäuser, we find that the clusters have almost the same structures although the PW model used by Kerner and Konhäuser has a viscous term. In this paper, the structure of transition layers is described by a

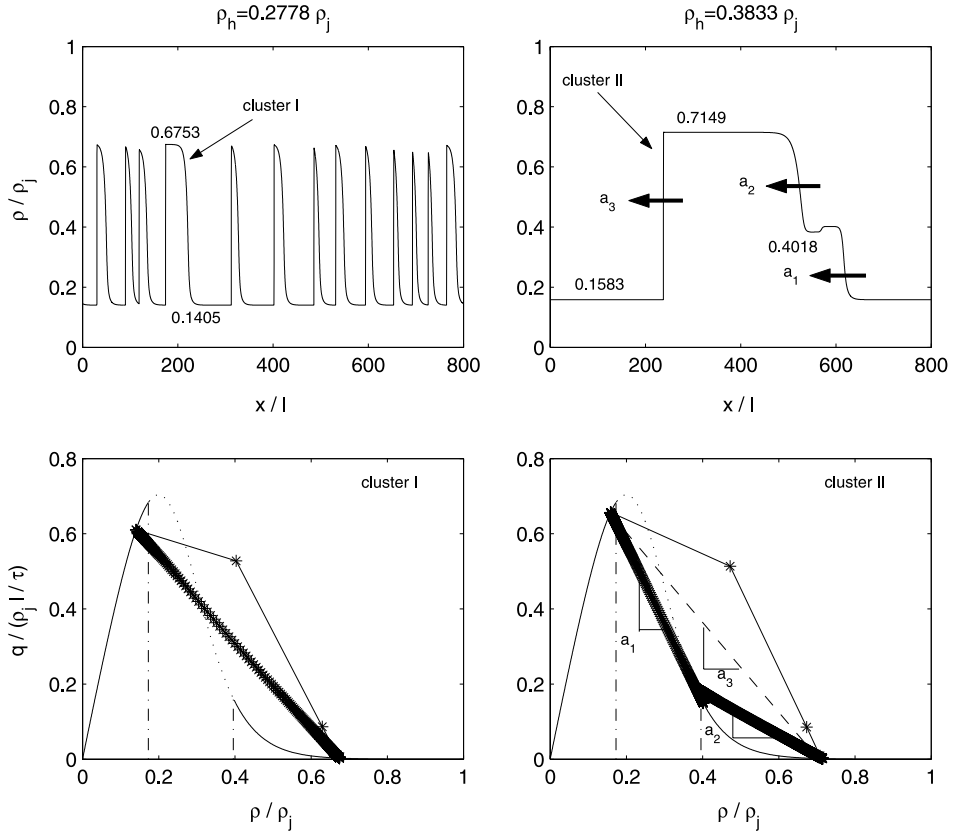

Fig. 14. Solutions with different initial traffic density ρ_h at 500τ for (8) with $\Delta\rho_0 = 0.0167\rho_j$ and $N = 6400$.

first-order ordinary differential equation, while Kerner and Konhäuser derived a much more complicated second-order equation. The numerical solutions, however, suggest that the two equations have similar solutions.

In this paper, numerical investigations are based on the fundamental diagram suggested by Kerner and Konhäuser, for which the singular point of (17) coincides with one of its three poles. For other fundamental diagrams, e.g. Newell's (1993) model, we expect that the structure of clusters will be different. Our study also reveals that the parameter c_0 is intricately related to the structure of vehicle clusters. Therefore one can use the cluster solutions to calibrate c_0.

References

Courant, R., Friedrichs, K., Lewy, H., 1928. ber die partiellen differenzengleichungen der mathematischen physik. Math. Ann. 100, 32–74.

Godunov, S.K., 1959. A difference method for numerical calculations of discontinuous solutions of the equations of hydrodynamics. Mat. Sb. 47, 271–306 (in Russian).

Herrmann, M., Kerner, B.S., 1998. Local cluster effect in different traffic flow models. Physica A 255, 163–198, Computational Physics, vol. 126, No. 2. Academic Press, 1996, pp. 449–467.

Jin, W.L., Zhang, H.M. Solving the Payne–Whitham traffic flow model as a hyperbolic system of conservations laws with relaxation (submitted to Transport. Res.).

Kerner, B.S., Konhäuser, P., 1994. Structure and parameters of clusters in traffic flow. Phys. Rev. E 50 (1), 54–83.

Lighthill, M.J., Whitham, G.B., 1955. On kinematic waves. II. A theory of traffic flow on long crowded roads. Proc. R. Soc. 229 (1178), 317–345.

Liu, T.P., 1987. Hyperbolic conservation laws with relaxation. Commun. Math. Phys. 108, 153–175.

Newell, G.F., 1993. A simplified theory of kinematic waves in highway traffic, part I. General theory. Transport. Res. B 27 (4), 281–287.

Payne, H.J., 1971. Models of freeway traffic and control. In: Mathematical Models of Public Systems. In: Simulation Councils Proc. Ser., vol. 1, pp. 51–60.

Richards, P.I., 1956. Shock waves on the highway. Operations Res. 4, 42–51.

Schochet, S., 1988. The instant response limit in Whitham's nonlinear traffic model: uniform well-posedness and global existence. Asymptotic Anal. 1, 263–282.

Whitham, G.B., 1959. Some comments on wave propagation and shock wave structure with application to magnetohydronamics. Commun. Pure Appl. Math. XII, 113–158.

Whitham, G.B., 1974. Linear and Nonlinear Waves. John Wiley and Sons, New York.

Zhang, H.M., 1999. An analysis of the stability and wave properties of a new continuum theory. Transport. Res. B 33 (6), 387–398.